Soil Dynamics and Earthquake Engineering 65 (2014) 224–242

Contents lists available at ScienceDirect

Soil Dynamics and Earthquake Engineering

journal homepage: www.elsevier.com/locate/soildyn

Cyclic response of masonry infilled RC frames: Experimental results and simplified modeling

Liborio Cavaleri*, Fabio Di Trapani

Dipartimento di Ingegneria Civile, Ambientale, Aerospaziale e dei Materiali (DICAM), University of Palermo, Viale delle Scienze, 90128 Palermo, Italy

ARTICLE INFO

Article history:
Received 4 May 2013
Received in revised form
19 March 2014
Accepted 7 June 2014

Keywords:
Infilled frames
Masonry infills
Cyclic behavior
Pivot hysteretic model
Equivalent strut

ABSTRACT

The recent large interest in nonlinear seismic analysis methods, static and dynamic, has required proper strategies of modeling based on reliable, and at the same time easy to use, constitutive laws for the structural elements. Regarding the behavior of framed structures, special attention has to be devoted to infills because of the key role they play in modifying overall stiffness, strength and ductility under seismic excitation. Pointing out the attention on this topic the paper discusses a criteria for modeling the structural behavior of infills based on a macromodeling approach, that is to say on the substitution of infills with diagonal pin jointed struts. Is here shown how multilinear plastic link elements governed by a hysteretic Pivot model, available in different FEM codes, can be appropriately used to model the equivalent struts to perform linear or nonlinear analyses. In order to enlarge experimental knowledge on cyclic behavior of infilled frames structures and as reference for developing the above mentioned modeling strategy, an experimental campaign on single-storey, single-bay, fully infilled frames with different kinds of masonry and subjected to lateral cyclical loads, was carried out, and some others available in the literature are referred to. Validation of Pivot modeling approach was carried out comparing experimental results and computer simulations of the experimental tests. In the paper hysteresis parameters values calibrating Pivot law are also given for involved masonry infills typologies and some proposals for correlation between strength and stiffness of infilled frames and of masonry infills are provided as a tool for the quick calibration of the Pivot model in practical applications.

1. Introduction

Reinforced concrete framed structures, infilled with masonry panels, are widespread and commonly employed in worldwide building traditions. The observation of post-seismic damage for these buildings shows that interaction between masonry infills and frames has a significant role in seismic response and global capacity that may or may not be beneficial. This role is often strongly dependant on regularity in plane and elevation infill distribution. A regular distribution of infills generally implies, especially for non-seismic designed buildings, a beneficial effect, increasing global bearing capacity and stiffness under lateral actions. On the other hand, irregular distributions of panels may be dangerous, often being the cause of additional torsional effects, in the case of planar irregularities, and of soft-storey mechanisms in the case of elevation irregularities.

Many authors have provided experimental and analytical studies proposing modeling strategies to predict interaction effects between frames and infills, suggesting micromodeling or macromodelling approaches. The latter, based on replacing each masonry infill with one or more equivalent pin-jointed struts, is more frequently employed in order to perform nonlinear static or dynamic analyses. Really this approach guarantees simplicity and a lower computational effort with respect to the micromodelling approach (based on the discretization of infills by finite elements). American technical codes [1] also suggest the macromodelling approach for seismic assessment of infilled framed structures, proving the suitability of this strategy.

The identification of an equivalent diagonal strut (Fig. 1), besides the attribution of geometrical characteristics, requires the assignment of specified mechanical characteristics for the infilled frame system which, especially for masonries constituting infills, are not always easy to predict. The quantity of required information depends also on the assessment approach (e.g. linear or nonlinear analysis) which is necessary to carry out. For a complete identification of the equivalent strut it is generally necessary to determine: (a) the initial stiffness, (b) the peak strength, and (c) the constitutive law shape (monotonic or cyclical).

The first studies on this topic are due to Holmes [2] who proposed replacing the panel with an equivalent diagonal strut, having cross-section width w equal to 1/3 of the diagonal length d. Other researchers followed with approaches based on the ratio between

* Correspondence to: Dipartimento di Ingegneria Civile, Ambientale, Aerospaziale, dei Materiali (DICAM), Università degli Studi di Palermo, Viale delle Scienze, 90128 Palermo, Italy. Tel.: +39 091 23896709.
E-mail address: liborio.cavaleri@unipa.it (L. Cavaleri).

http://dx.doi.org/10.1016/j.soildyn.2014.06.016
0267-7261/

the elastic characteristics of the infill and the surrounding frame for the identification of the equivalent strut cross-section width [3–8]. In a more recent study Papia et al. [9] proposed an identification technique that introduces the dependence of the strut width not only on the stiffness ratios between frame and infill but also on the mechanical elastic properties of the infill along the diagonal direction. Subsequently, the dependence on the vertical load transmitted by the frame to the infill was introduced by Amato et al. [10,11], while an alternative method, based on a dynamic structural identification strategy, was suggested and proposed for a number of cases in [12–15].

With regard to the definition of a constitutive law for equivalent strut, the study by Panagiotakos and Fardis [16] should also be mentioned. There, the yielding force corresponding to the first cracking of an infill is determined depending on the tensile strength of the masonry of which it is made evaluated by diagonal compressive tests. Bertoldi et al. [17] proposed to choose the maximum strength of a strut depending on the possible failure mechanisms for the equivalent infill panel.

More relevant to the aims of this paper, in which cyclic behavior of infilled frames structures is dealt with, are some experimental and analytical works, such as that by Klingner and Bertero [18] which investigated the effects of cyclic loads by testing portions of multi-storey buildings, also providing a first hysteretic model. Doudoumis and Mitsopoulou [19] introduced in their hysteretic model an initial non-loading branch due to shrinkage of contact zones. Experimental pseudo-dynamic tests on masonry infilled RC frames were carried out by Mander et al. [20,21] and Mehrabi et al. [22] who also provided a cyclic law based on the results of tested infilled frames specimens. Other hysteretic models were further proposed, each of them based on different assumptions. Madan et al. [23] proposed a hysteretic single-strut model taking into account strength and stiffness decay and pinching, Crisafulli [24] investigated the influence of different multiple-strut models on structural response, Kappos et al. [25] presented a hysteretic model based on shear strength of infills. In the last years Cavaleri et al. (2005) [26] proposed a highly detailed constitutive law for cyclical or monotonic behavior of an equivalent single strut and provided a first calibration of the parameters involved, while Crisafulli and Carr [27] developed a new multi-strut macro-model including, in addition to classical truss elements, governed by

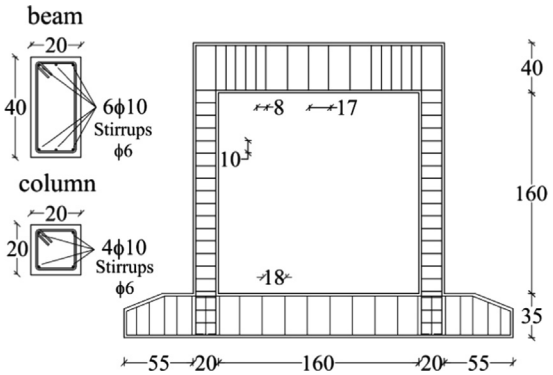

Fig. 2. S1A and S1B specimen details (measures in cm).

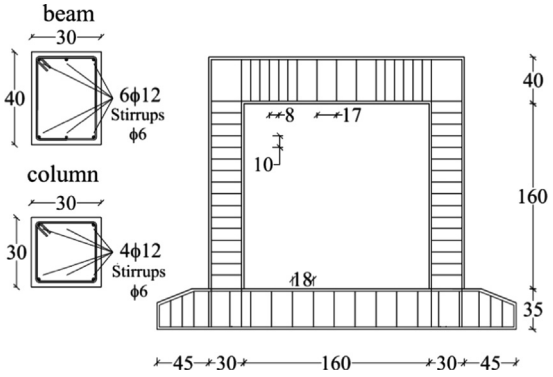

Fig. 3. S1C specimen details (measures in cm).

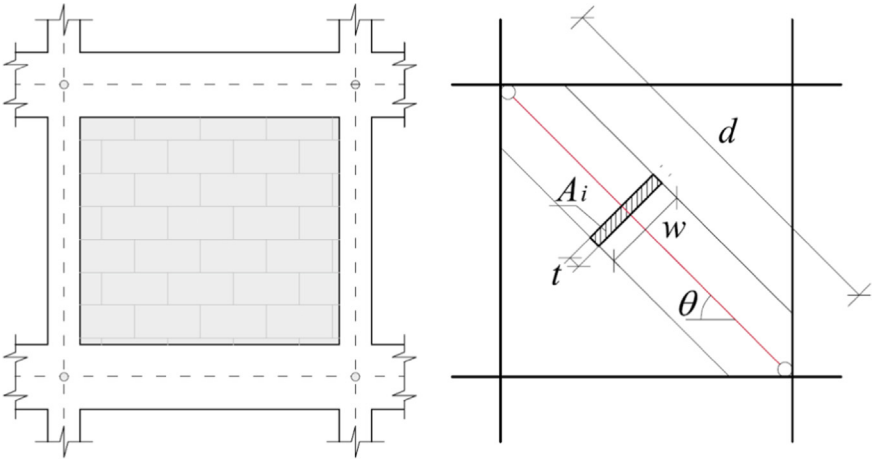

Fig. 1. Equivalent diagonal single strut definition and geometrical characteristics.

Table 1
Specimen geometrical characteristics description.

Code	Masonry infill	No. of specimens	Column dimensions (cm)	Beam dimensions (cm)	
S1A	Calcarenite masonry	2	20 × 20	20 × 40	Actual investigation
S1B	Clay masonry	2	20 × 20	20 × 40	
S1C	Lightweight concrete masonry	4	30 × 30	30 × 40	
S2A	Calcarenite masonry	2	20 × 20	20 × 40	Previous investigation
S2B	Clay masonry	2	20 × 20	20 × 40	

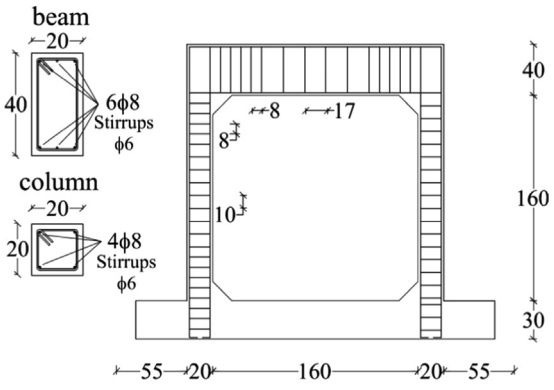

Fig. 4. S2A and S2B specimen details (measures in cm).

axial compressive laws, a special shear spring to account for frictional effects. An extensive state of the art of mathematical macromodels for infilled structures is provided by Asteris et al. [28] including a proposal for the stiffening effect of brick masonry infills [29].

Among the above mentioned models, those including the cyclic behavior often depend on a large number of parameters, making it difficult to use them for practical applications. The problem becomes more relevant in the case of multiple-strut configurations (double, triple pin jointed struts or mixed axial and shear struts) without considering the different possible infill/frame couplings, which introduce further uncertainties. However, the necessity to assess the capacity of existing structures is today increasing, and as several studies demonstrate [30–34]. The analyses should be adequately performed including infill panels to avoid underestimation or overestimation of buildings' actual capacities.

Table 2
Mechanical properties of masonry employed to arrange infills.

Calcarenite masonry	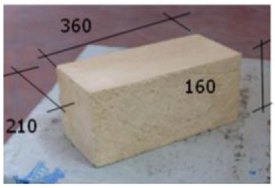			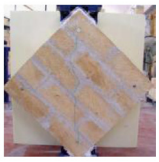
S1A	Mortar - f_m=3.06 Units - f_{bm}=7.06	E_2=3933 f_m=2.67	E_1=7408 f_m=3.08	G_{12}=1348 $_{12}$=0.22 $_{21}$=0.10 f_{vm}=0.73
S2A	Mortar - f_m=9.89 Units - f_{bm}=4.00	E_2=7106 f_m=4.57	E_1=9528 f_m=3.92	G_{12}=2937; $_{12}$=0.10 $_{21}$=0.085 f_{vm}=0.89
Clay masonry	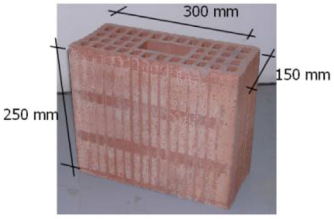			
S1B-S2B	Mortar - f_m=9.16 Units - $f_{bm,v}$=37.68 $f_{bm,h}$=2.06	E_2=6401 f_m=8.66	E_1=5038 f_m=4.18	G_{12}=2547 $_{12}$=0.07 $_{21}$=0.09 f_{vm}=1.07
Lightweight concrete masonry	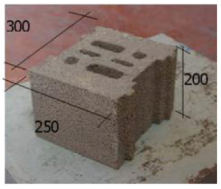			
S1C	Mortar - f_m=9.57 Units - $f_{bm,v}$=4.07 $f_{bm,h}$=3.15	E_2=4565 f_m=1.74	E_1=1944 f_m=0.30	G_{12}=2042 $_{12}$=0.13 $_{21}$=0.22 f_{vm}=0.29
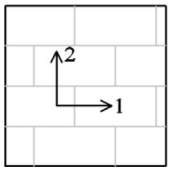 Masonry mechanical properties reference system				

The introduction of the infill panel contribution thus appears absolutely necessary as does the adoption of simplified models, also not too heavy from the computational point of view. In this context the paper has the aim of discussing how the cyclic behavior of infilled frames can be predicted with sufficient accuracy by modeling equivalent diagonal struts by means of multilinear plastic link elements, available in the libraries of different FEM codes, governed by the *Pivot hysteretic law* proposed by Dowel et al. [35].

First an experimental campaign, involving single-storey-single-bay frames infilled with different types of masonry, is discussed. Then the experimental cyclic responses of the before mentioned frames is analyzed in order to recognize the possibility of modeling them by the Pivot hysteretic law, whose characteristics give no few computational advantages for the practical applications.

2. Experimental investigation

An enlargement of the experimental knowledge about the cyclic behavior of RC frames arranged with different kinds of masonry infills is provided in this paper. Two experimental campaigns on single-storey, single-bay RC fully infilled frames are discussed and furthermore used to prove the suitability of the Pivot hysteretic model as an instrument for the assessment of the overall behavior of RC masonry infilled structures when nonlinear time history analyses should be performed.

The masonries selected for the execution of the experimental tests (arranged with calcarenite blocks, clay blocks, and lightweight concrete blocks) represent three main traditional typologies used to realize infill panels. It is clear that each kind of masonry may present several sub-typologies in real cases therefore the data here

Fig. 6. Hollow hydraulic jacks for vertical load application.

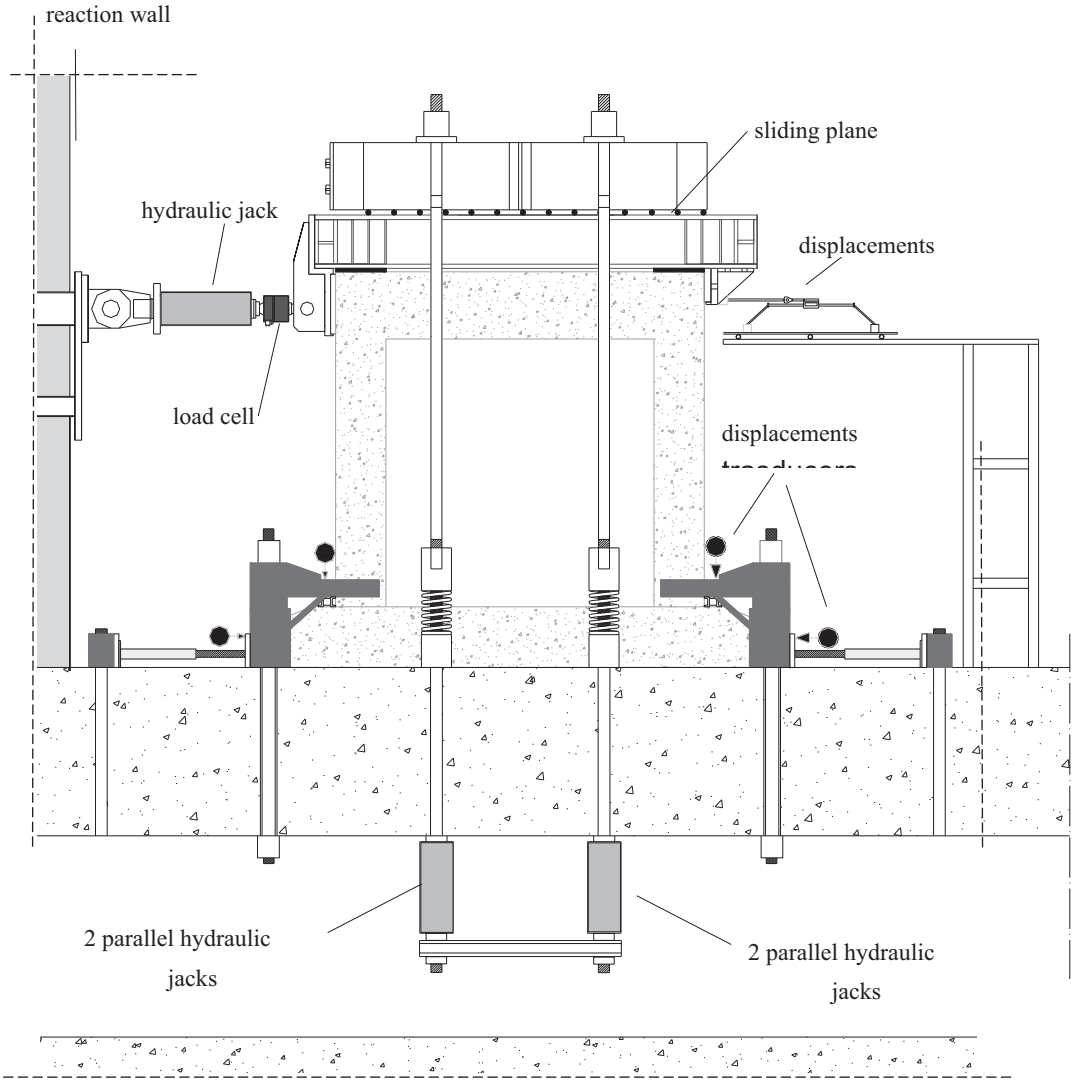

Fig. 5. Test set up.

presented constitute only a part of the whole possible results for each masonry infill typology.

2.1. Specimen characteristics

The experimental campaigns were carried out at two different times. Regarding the more recent, experimental program included 8 infilled frames (S1 series) designed to represent a typical configuration recognizable in existing buildings designed for gravity loads and without any seismic detail. Geometrical ratios between beam and column cross-sections define a weak column-strong beam scheme. The ratio between the bay length and the storey height was approximately 1. Specimens were arranged with three different kinds of masonry among the most widespread in practical applications: 2 specimens were infilled with calcarenite masonry (S1A specimens), 2 with clay masonry (S1B specimens), and 4 with lightweight concrete masonry (S1C specimens). The mean concrete strength, measured after 28 days, was 25 MPa, while the elastic Young modulus was about 25,500 MPa. The reinforcement steel bars had a medium strength of 450 MPa. The typological characteristics of the specimens are summarized in Table 1.

Experimental results and geometrical details for 4 additional infilled (S2 series) frame specimens, tested in a previous experimental campaign [26], are also considered here in order to enhance the data and comparing the results. Among these four frames two were infilled with clay masonry and further two with calcarenite masonry. The mechanical characteristics of concrete and rebars were similar to those previously mentioned. The details of the first and second series of specimens with the specifications of the reinforcements are reported in Figs. 2–4.

The masonries used to arrange the specimens were preliminarily subjected to experimental tests in order to assess their mechanical properties. Ordinary, lateral and diagonal compressive tests were carried out. Compressive tests on mortars and units (in both orthogonal directions) were also performed. This preliminary experimental campaign is exhaustively discussed in Cavaleri et al. [36].

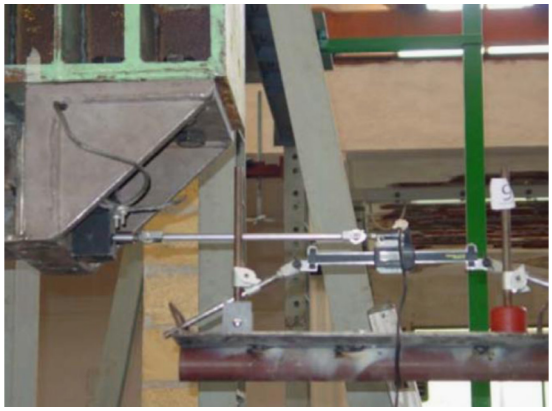

Fig. 9. Transducer for the top lateral displacement measuring.

Fig. 10. A specimen in the test apparatus.

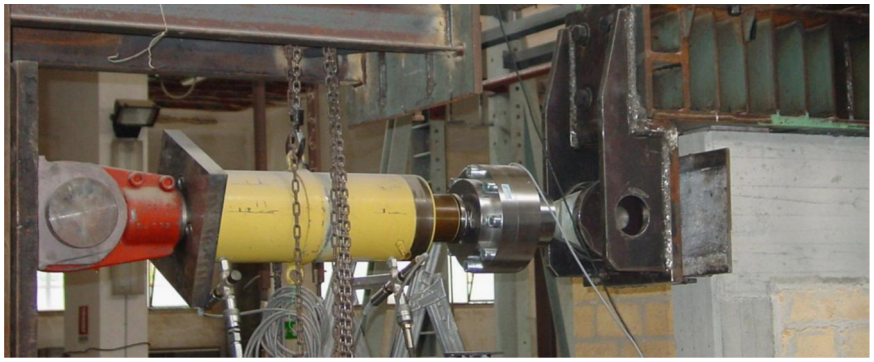

Fig. 7. Hydraulic jack for lateral load application.

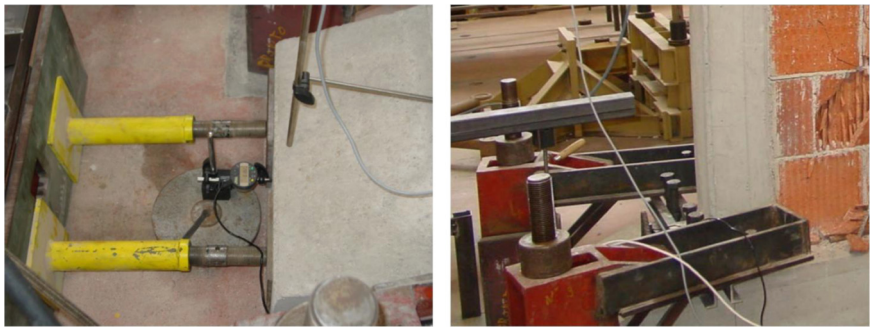

Fig. 8. Specimen translation and rotation constraints.

All the significant results in terms of mechanical elastic properties and strengths are summarized in Table 2.

2.2. Test setup and instrumentation

The test setup is shown in Fig. 5. Specimens were primarily subjected to an axial vertical constant load (200 kN on each column), applied by four manually controlled hollow hydraulic jacks (Fig. 6). The device for the application of the vertical load was constrained with respect to the horizontal displacement in order to maintain the verticality and to permit free sliding of the head of each frame. The resulting force applied was monitored by measuring the oil pressure in the jacks. Lateral loads were applied by a horizontal double-acting jack (Fig. 7) monitored by a load cell, having a 500 kN capacity, interfaced with the acquisition system. A special system of constraints was provided at the base of the specimens to avoid rigid translations and rotations (Fig. 8).

The displacements at the top of each specimen were measured by means of a transducer having measuring range 0–200 mm (Fig. 9). In addition to the lateral displacement of each frame head, the horizontal displacement and the rotation (in the plane of each frame) of the base were monitored by 4 digital gauges having measuring range 0–12.5 mm; in this way constraining efficacy was verified. In Fig. 10 a real view of a specimen in the test apparatus is shown.

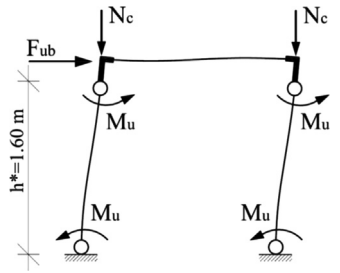

Fig. 11. Simplified scheme for the evaluation of the lateral strength of bare frames.

Table 3
Plastic moments of columns cross sections, analytical lateral strength and experimental lateral stiffness of bare frames.

	M_u [kN m]	F_{bu} [kN]	K_b experimental average [kN/mm]
SIA-S1B	24	60	11
S1C	48	120	43
S2A-S2B	22	55	–

2.3. Bare frames

The stiffness of the bare frames was measured before the infills were made for a further comparison with the one owned by the infilled frame specimens. Once it was recognized that flexural mechanisms anticipate shear mechanisms, the strength of the bare frames was predicted by a simplified model corresponding to a limit equilibrium associated with the plasticization of the top and base sections of columns. In calculating the ultimate moments of the columns M_u, the axial load N_c (200 kN) on the columns

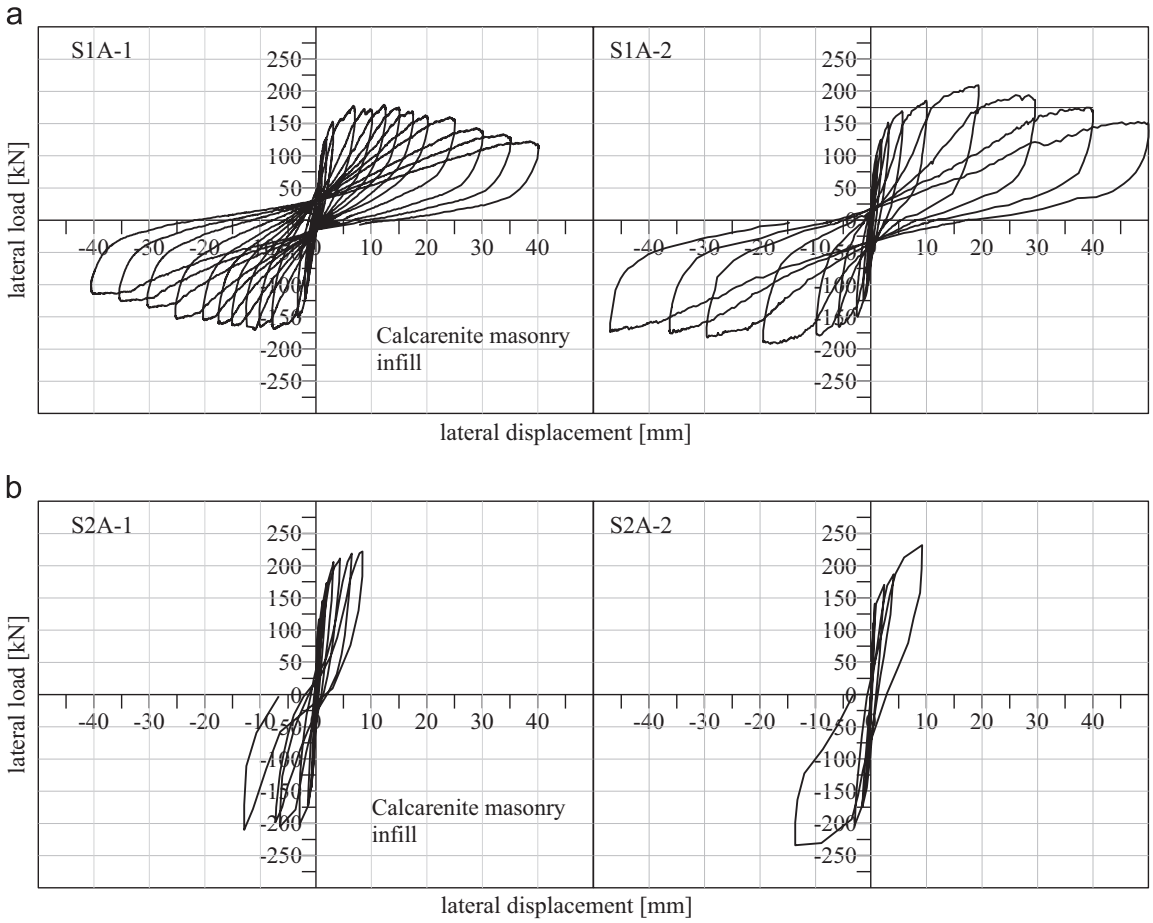

Fig. 12. Force–displacement experimental curves of calcarenite masonry infilled specimens: (a) S1 ; and (b) S2 series.

themselves was taken into account. Referring to Fig. 11, the bare frame strength F_{ub} was evaluated by the limit equilibrium condition leading to the following expression:

$$F_{ub} = \frac{4M_u(N_c)}{h^*} \quad (1)$$

in which h^* is the net height of each bare frame.

The predicted values of the lateral strengths for the S1 and the S2 series are reported in Table 3. In the same table the values of the mean experimental stiffness are inserted.

2.4. Cyclic response of infilled frames and remarks regarding the modeling

The specimens of S1 series were tested by increasing the displacement at each cycle up to a drift of 2.5 %. The cycle amplitude increment was variable during the loading pattern up to a maximum of 10 mm for the last cycles. Damage mechanisms were monitored during the tests in order to detect propagation of cracks on infills and frames. Stiffness, strength, and ductility evaluations were carried out. The specimens of S2 series were tested up to a drift of 0.6%. The cyclic responses for the specimens of S1 and S2 series are reported in Figs. 12–14.

In terms of maximum average lateral strength, calcarenite and clay masonry infilled specimens showed a global increase of about 3.4 times compared to the corresponding bare frames. Lightweight concrete masonry infills had a lower, but not negligible, influence on strength, showing an increase of about 2.2 times. This was first due to a lower shear strength, which is typical of this kind of masonry.

A low strength degrading after peak reaching was observed for all specimens, demonstrating an efficient confinement effect produced by the frames on the infill panels. For the specimens of S1 series a significant loss of strength was observed only after a drift of 1.8%.

Cracking propagation affected both frames and infills. First, approximately diagonal cracks formed on frames at the upper joints close to the columns (Fig. 15). These cracks revealed the weakness of the joints with respect to the strength of the critical regions of columns and beams. This is usual in the existing structures, however joints maintained the capacity to reciprocally transmit stresses from one RC member to another and from infill to RC members. With regards to the modeling of what observed, when the strategy of substitution of infill with an equivalent strut is adopted, the non exact correspondence between the real state evolution (e.g. cracking pattern, failure modes, etc.) and the model structural state is generally accepted as long as a match, by the global phenomenological point of view, is recognized [37] (e.g. in lateral stiffness, in lateral strength, in degradation of stiffness and strength, in residual strength, etc). This is the natural consequence of the substitution of a substructure (namely an infill) with a deeply different element (namely a strut). Therefore, the behavior observed was effectively modeled supposing the formation of plastic hinges at the ends of columns and calibrating an equivalent strut able to match the global phenomenon.

Diagonal cracks corresponding to those occurred at the beam–column joints affected infills mainly following mortar joints.

For larger displacements (over 20 mm) more evident cracking propagation, corresponding to the beginning of strength decay,

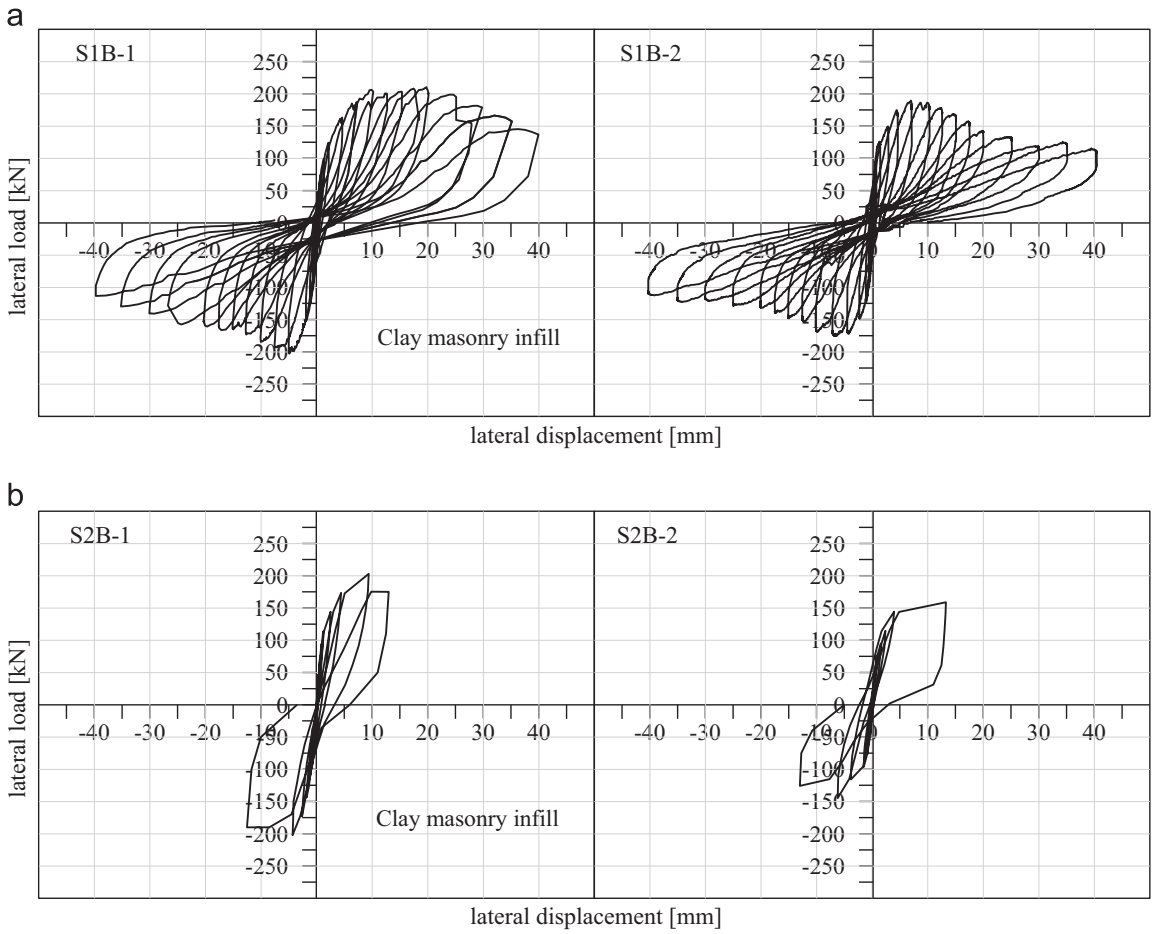

Fig. 13. Force–displacement experimental curves of clay masonry infilled specimens: (a) S1 ; and (b) S2 series.

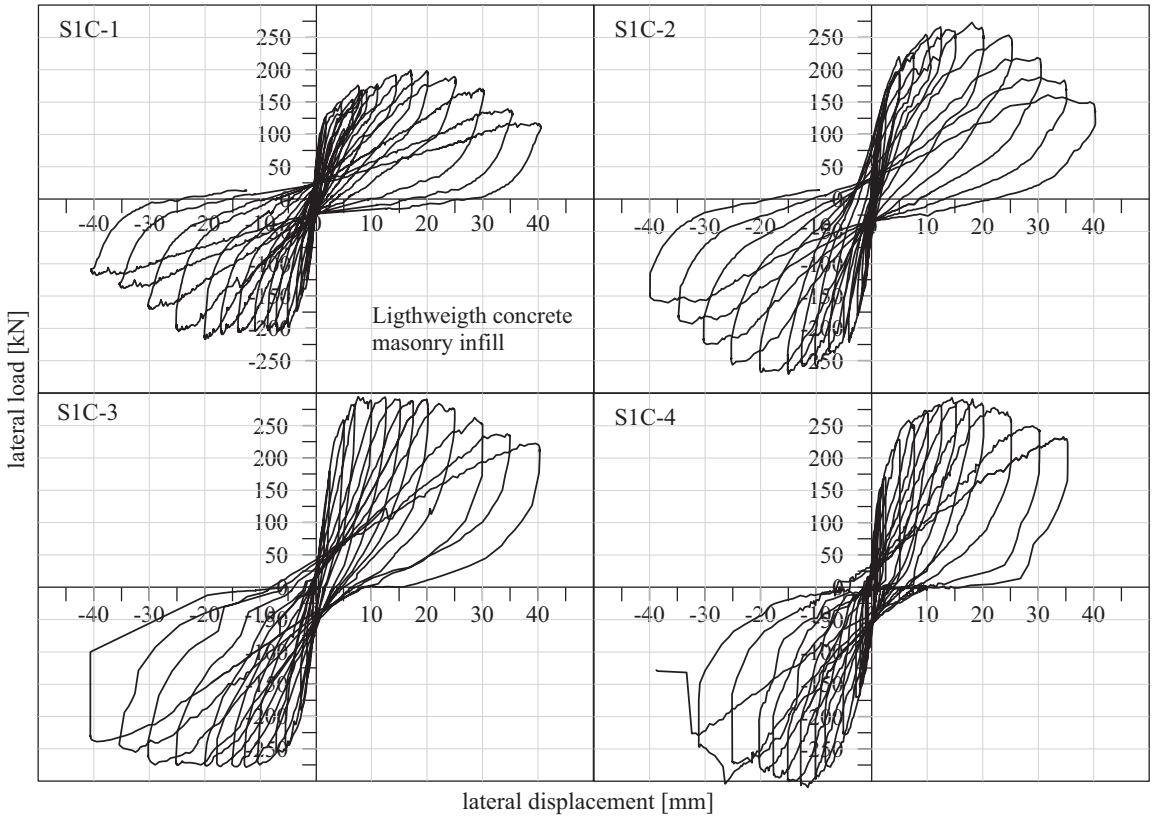

Fig. 14. Force–displacement cyclical test results for lightweight concrete infilled specimens. S1 series.

Fig. 15. End of column and beam–column joint damaging.

was observed accompanied by the formation of sub-horizontal cracks in the middle of columns and more severe damage at beam column joints (Fig. 15).

Also in this case a simplification able to capture the global response was adopted: the cracks at the middle height of columns were not associated to a damage in the column model but this was included in the possibility of formation of plastic hinges at the downer critical regions.

Clay and lightweight concrete masonry infills were affected by partial crushing of the units placed at the corners and along the two diagonal directions while more diffused cracking patterns were recognized on calcarenite masonry infills. This is a proof of a good global capacity of stress redistribution. In Fig. 16, some infilled frame specimens at the end of tests with the cracking patterns detected are shown.

With regards to stiffening effects, specimens infilled with calcarenite and clay masonry showed the most significant increment, exhibiting respectively an average increase of 8.3 and 11.4 times. Lightweight concrete masonry infills showed instead a lower influence on overall stiffness: in this case an increment of 1.9 times compared to the bare frames was recorded. However all specimens exhibited a significant stiffness degradation at each cycle, especially after the peak strength was reached. On the other hand the peak strength did not significantly decrease until large displacements occurred. Cyclic experimental curves showed a significant pinching effect at load reversal for all tested specimens. This was mainly consequence of the infill crack closure and was much more marked as the crack pattern was more extended.

Ideally enveloping the cycles of the responses, global ductile behavior was observed, though the collapse of the whole system

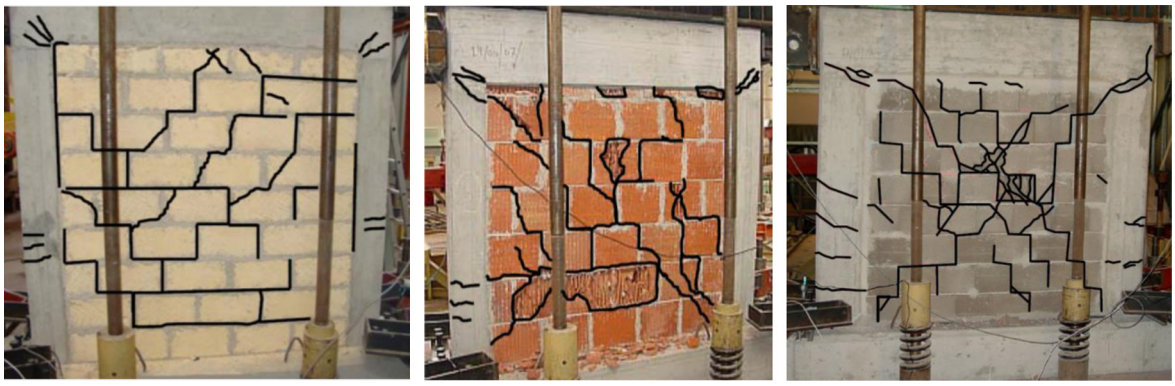

Fig. 16. Typical specimen cracking patterns at the end of the tests.

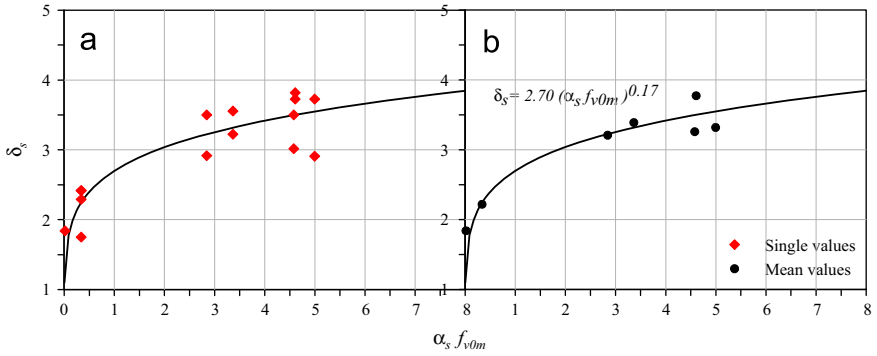

Fig. 17. δ_s–$\alpha_s f_{v0m}$ correlation: (a) values of δ_s referred to each specimen; and (b) mean values of δ_s referred to each typology of specimens.

was governed by the failures of the columns not clearly recognizable as ductile.

2.5. Considerations on strength increment due to infills

As shown by the experimental results, infill panels play a major role in global strength and stiffness. Regarding the strength of the specimens tested, an increase of 2–4 times compared to the bare frames was detected for the different infill typologies.

It is not simple to predict the global strength of infilled frames, which depends on the degree of coupling between frame and infill and involves a high numbers of variables. Nevertheless, the strength of infilled frames is important for the definition of adequate mechanical properties for the struts equivalent to infills. As well exposed in the subsequent sections, in order to attribute for each case a monotonical constitutive law, representing the backbone curve for the Pivot model, may be useful the definition of a tool being able to predict the strength of an infilled frame. For this purpose it is possible to establish, basing on experimental results, a correlation between global strength increment and frame/infill mechanical properties. If one defines the strength increment ratio δ_s due to infill as

$$\delta_s = \frac{F_{ui}}{F_{ub}}, \tag{2}$$

in which F_{ui} is the maximum strength exhibited by an infilled frame and F_{ub} is the correspondence bare frame lateral strength, an expression for δ_s, including the mean shear strength f_{v0m} of masonry infills, can be established. By observing the experimental results reported in Fig. 17, the best fitting law for δ_s can be obtained as

$$\delta_s = 2.75(\alpha_s f_{v0m})^{0.17} \tag{3}$$

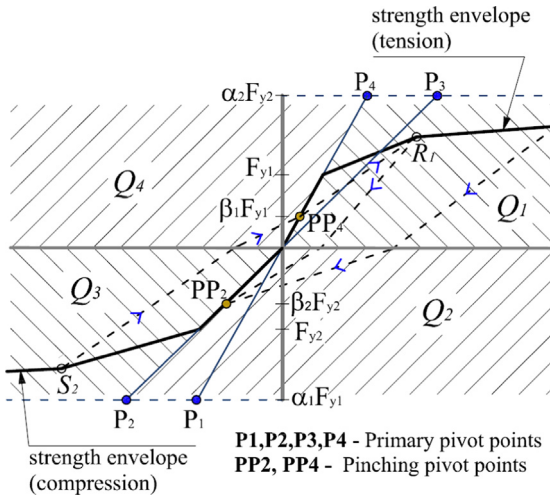

Fig. 18. Hysteretic Pivot model for a generic unsymmetrical tension–compression law.

where the parameter α_s is expressed as

$$\alpha_s = \frac{F_{up}\cos\theta}{F_{ub}} \tag{4}$$

θ being the angle defining the slope of the frame diagonal while F_{up} represents a conventional infill diagonal strength, classically obtained as

$$F_{up} = f_{v0m} t d \tag{5}$$

t being the infill thickness and d the length of infill diagonal.

As noticeable in Fig. 18, single and mean experimental values appear fairly condensed around this proposed correlation law

Table 4
Strength values exhibited by specimens varying shear strength of panels and infill/frame strength ratios.

Spec. code	Infill units	f_{v0m} [Mpa]	F_{ub} [kN]	F_{ui} [kN]	δ_s	δ_s mean	$f_u \cos\theta$ [kN]	α_s	$\alpha_s f_{v0m}$ [Mpa]
S1A-1	Calcarenite	0.73	60	175.0	2.92	3.21	233.6	3.89	2.84
S1A-2	Calcarenite	0.73		210.0	3.50		233.6		
S1B-1	Clay	1.07	60	210.0	3.50	3.26	256.8	4.28	4.58
S1B-2	Clay	1.07		181.0	3.02		256.8		
S1C-1	LW conc.	0.29	120	210.0	1.75	2.22	139.2	1.16	0.34
S1C-2	LW conc.	0.29		275.0	2.29		139.2		
S1C-3	LW conc.	0.29		290.0	2.42		139.2		
S1C-4	LW conc.	0.29		290.0	2.42		139.2		
S2A-1	Calcarenite	0.89	55	210.0	3.82	3.77	284.8	5.18	4.61
S2A-2	Calcarenite	0.89		205.0	3.73		284.8		
S2B-1	Clay	1.07	55	205.0	3.73	3.32	256.8	4.67	5.00
S2B-2	Clay	1.07		160.0	2.91		256.8		
Ref. [28]	Clay bricks	0.08	–	–	1.84	1.84	7.0	0.19	0.02
Ref. [33]	Clay bricks	0.80	180	640	3.56	3.39	757.0	4.21	3.36
Ref. [33]	Clay bricks	0.80	180	580	3.22		757.0	4.21	3.36

which expresses substantially that the overall strength increment depends not only on the shear strength of infills but is significantly modulated by the infill–frame strength ratio α_s.

The experimental values employed for the construction of these analytical relationships include the results of the S1 and S2 series of specimens and also the strength values reported in Kakaletsis et al. [31] and Koutromanos et al. [38] who tested different typologies of brick masonry infills. In Table 4 the strength values and detected ratios are summarized.

A simple way to use the above correlation for providing and estimating the equivalent diagonal strut peak strength is discussed afterwards.

2.6. Ductility

Considering the strength envelopes of the experimental cyclic responses a global ductile behavior can be observed. The strong nonlinearity of the initial branch and the low slope of the softening branches make it difficult to exactly identify the yielding and ultimate displacements to calculate the ductility factor.

As suggested in [31] a conventional ductility factor $\mu_{0.85}$ can be defined drawing a horizontal straight line at 85% of the peak strength, intersecting the envelope at two points, one on the ascending and one on the descending branch. The ductility strength envelope factor $\mu_{0.85}$ is calculated as the ratio between the displacements corresponding to these two points. Further the specimen ductility factor is the mean value of the two $\mu_{0.85}$ ductility factors evaluated for the positive and negative response envelopes of the same specimen. The ductility factors calculated for the tested specimens are reported in Table 5, where the mean ductility values are also shown for each infill typology. The values vary from 5.08 (clay masonry infilled specimens) to 7.61 (lightweight concrete masonry infilled specimens). An intermediate behavior was exhibited by the calcarenite masonry infilled specimens, for which the mean ductility factor is 6.15. It should be noticed that the lightweight concrete masonry infilled specimens, which showed the highest ductility values, were interested by a better confinement action of RC frames, whose members had larger dimensions.

From a general point of view the response recognized has shown that, though the failure of all infilled frame specimens was governed by crack patterns that were not exactly associable to ductile mechanisms, an overall ductile behavior was exhibited.

Table 5
Ductility factors.

	Infill of	$\mu_{0.85}$ positive envelope	$\mu_{0.85}$ negative envelope	$\mu_{0.85}$ mean	Mean ductility
S1A-1	Calcarenite	5.40	5.63	5.51	6.15
S1A-2	Calcarenite	6.67	6.92	6.79	
S1B-1	Clay	5.08	6.30	5.69	5.08
S1B-2	Clay	3.50	5.43	4.47	
S1C-1	LW conc.	5.88	12.00	8.94	7.61
S1C-2	LW conc.	5.50	6.98	6.24	
S1C-3	LW conc.	6.96	11.67	9.31	
S1C-4	LW conc.	6.00	5.88	5.94	

3. The "Pivot" model proposal for the equivalent strut modeling

3.1. Pivot hysteretic model

Many models have been developed to describe the cyclic nonlinear behavior of diagonal struts equivalent to infills. However, in order to perform dynamic nonlinear analyses for complex RC masonry infilled frame structures, flexible instruments requiring few parameters and a low computational effort, accompanied by sufficient reliability in the results, appear to be necessary.

The use of the *Pivot hysteretic model* was first proposed by Dowel et al. [35] as an instrument to predict hysteretic behavior of RC columns under cyclic actions. The aim was to simplify the computational effort required by classical fiber numerical analysis of cross sections. The same authors suggested this model to reproduce force–displacement laws in general. The advantage of using the Pivot model is essentially due to the fact that this model is based mainly on geometrical rules that define loading and unloading branches rather than analytical laws. This reduces not only the computational effort but also the number of hysteretic parameters involved. Moreover, the Pivot model has great flexibility in modeling unsymmetrical tension–compression behaviors, as in the case of infill equivalent struts which are considered resistant only to compression stresses. An absolutely general outline of Pivot model is reported in Fig. 18. The model is completely defined when tension and compression strength envelopes are attributed (yielding tension and compression values F_{y1} and F_{y2}, initial stiffness and peak strength). Hysteresis rules are governed by parameters α_1, α_2, β_1 and β_2. Their significance is expounded below, with a brief summary of the Pivot model.

By the intersection of the horizontal lines through the ordinate values $\alpha_2 F_{y2}$, $\alpha_1 F_{y1}$, $\beta_1 F_{y1}$ and $\beta_2 F_{y2}$ and the lines containing the initial elastic branches, the primary Pivot points P_1, P_4 and P_2, P_3 and the Pivot pinching points PP_2 and PP_4 are identified. The quadrants Q_1, Q_2, Q_3 and Q_4 are delimited by the abscissa axis and the initial elastic branches defined before.

Starting a cycle from Q_1 (tension), once the yielding value is exceeded the unloading branch is directed toward the point P_1 in Q_1 quadrant and toward the pinching Pivot point PP_2 in the Q_2 quadrant until the initial elastic branch is reached. The cycle follows this branch (P_2 direction) up to the compression yielding stress. Beyond this point the cycle is in the Q_3 quadrant where unloading goes toward the point P_3 and, after reaching Q_4, goes toward the pinching Pivot point PP_4 on the initial elastic tension branch. At this state the cycle restarts in the Q_1 quadrant toward the point R_1, which represents the last force value reached before

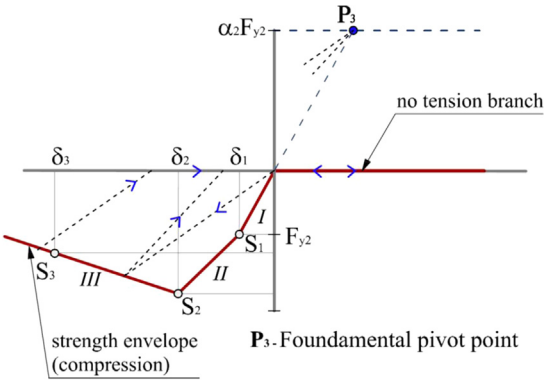

Fig. 19. Hysteretic Pivot law particularization for the equivalent diagonal strut.

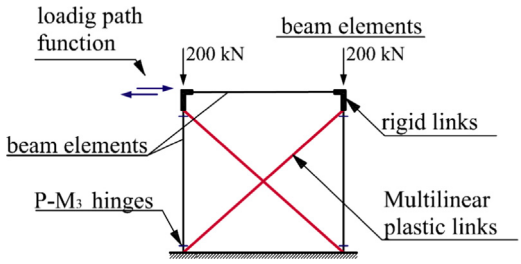

Fig. 20. Structural FEM model employed for the analyses.

the previous unloading in Q_1. The hysteresis parameters α_1, α_2, β_1 and β_2 should be appropriately fixed.

The application of the Pivot hysteretic model undergoes major simplification when applied to infill equivalent diagonal strut. In this case, since the infill panels do not offer any contribution in terms of tensile strength, the parameters α_1 and β_1 are null. Furthermore, experimental observation shows that infilled frame systems do not gain stiffness at load reversal until the whole plastic deformation (previously accumulated) is recovered. Basing on this hypothesis, the β_2 parameter is also null. The hysteretic law is therefore only governed by the α_2 parameter which is here experimentally calibrated for masonry infills which are object of the actual investigation. As reported in Fig. 19 a strong simplification is obtained with respect to the general case. The point P_3, which becomes the *fundamental Pivot point*, guiding unload directions is identified once yielding compression value F_{y2} and α_2 parameter are assigned. The points S_1, S_2 and S_3 on the compression envelope respectively represent the yielding, the peak and the restoring force corresponding to a reduction by 30% of the peak strength.

3.2. Definition of models of infilled frames

The reference structural model (Fig. 20) was formulated using SAP 2000 NL software. Beam elements for RC frame members were used. Taking into account the hierarchy in strength between columns and beams and the adequate shear strength of the members, mechanical nonlinearities of frame were introduced by means of four interacting axial load-moment plastic hinges placed at the ends of the columns. Beam–column joints were modeled as rigid links. Referring to plastic hinges, an elastic perfectly plastic envelope of the moment-curvature law was assigned with maximum moment and ultimate curvature obtained depending on the reinforcement and concrete characteristics (as a consequence of the stirrup confinement an ultimate strain for the concrete equal to 6‰ was fixed). The cyclic moment-curvature degradation was governed by a Takeda [39] law. The equivalent diagonal struts, representing the different kinds of infill panels, were modeled

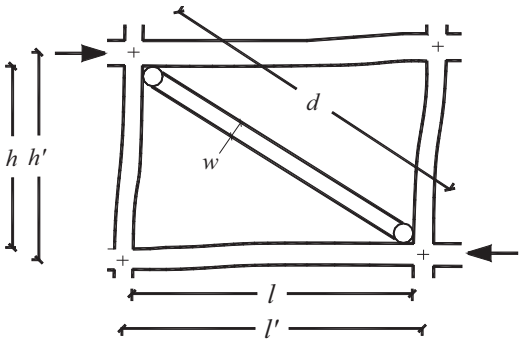

Fig. 21. Geometrical features of frame with strut equivalent to infill.

through *multilinear plastic link* elements for which the general Pivot model is implemented in SAP 2000 NL.

It is important to notice that the attribution of the strength envelope for the link elements, which guides the Pivot law, can be performed using any predictive model provided by the literature, therefore the afterwards discussed procedure constitutes only one of the alternatives.

In this case the initial stiffness was assigned through the expression proposed by Papia *et al.* [9], in which the cross-section height w is evaluated depending on the parameter λ^* that each time identifies the frame/infill system by means of the following expression:

$$w = dk\frac{c}{z}\frac{1}{(\lambda^*)^{\beta}} \tag{6}$$

where c and β depend on the Poisson's ratio ν_d of infill along the diagonal direction and can be evaluated as follows:

$$c = 0.249 - 0.0116\nu_d + 0.567\nu_d^2$$
$$\beta = 0.146 - 0.0073\nu_d + 0.126\nu_d^2 \tag{7}$$

The coefficient z takes on the value 1 since the panels are square ($l/h=1$) while the coefficient k depends on the level of the vertical loads acting on the columns, varying from 1 (negligible vertical loads) to 1.5 (high vertical loads). In this case k was set equal to 1.3 since and intermediate level of vertical loads was acting on the columns. A more accurate evaluation strategy for prediction of k is discussed in [10,11].

Finally, the parameter λ^* can be evaluated as

$$\lambda^* = \frac{E_d}{E_f}\frac{th'}{A_c}\left(\frac{h'^2}{l'^2} + \frac{1}{4}\frac{A_c}{A_b}\frac{l'}{h'}\right) \tag{8}$$

where E_d and E_f are respectively the Young modulus of the infill along the diagonal direction and the Young modulus of the frame concrete, A_c and A_b are the areas of the cross-sections of the frame columns and beams, while the geometrical features of the infill frame system t, l, l', h, h' are defined in (Fig. 21).

According to this formulation, the elastic moduli of masonry panels E_d and Poisson's ratios ν_d should be identified along the diagonal direction (along which the equivalent pin-jointed strut lies). The prediction of these values was carried out according to the strategy proposed by Cavaleri et al [40] which is based on the knowledge of the elastic properties E_1, E_2, G_{12}, ν_{12} of masonries along the two principal directions. These parameters are predictable starting from masonry strength along the same directions.

The peak strength S_2 of the equivalent struts can be fixed with one of the criteria available in the literature. Alternatively it can be iteratively determined by using the correlation (2) as discussed below.

If a prediction of the global strength of the infill/frame system F_{ui} is approximately performed as the sum of the bare frame strength F_{ub}, evaluated as in Eq. (1), and the horizontal component

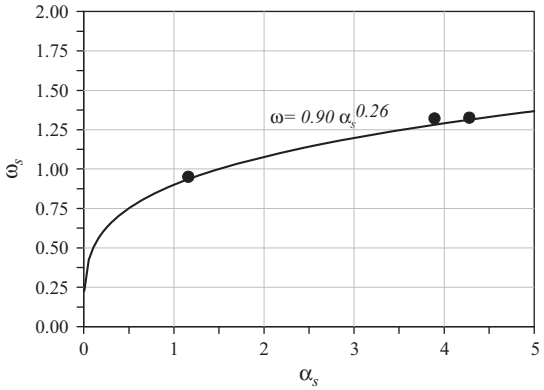

Fig. 22. ω_S–α_S correlation.

of the strut strength S_2^I, that is

$$F_{ui} = F_{ub} + S_2^I \cos\theta, \tag{9}$$

where the angle θ defines the slope of the diagonal strut, then by means of Eq. (9) an approximation of the equivalent strut strength can be obtained as

$$S_2^I = \frac{F_{ui} - F_{ub}}{\cos\theta} \tag{10}$$

Clearly Eq. (10) is only an approximate expression because (1) it is not certain that the collapse of the system will overlap the collapse of the frame and of the infill, and (2) the infilled frame strength is conditioned by the level of coupling between frame and infill so the collapse mechanism is more complex than a scenario in which the frame collapses as if it was bare and the infill collapses as if it was an axially loaded strut.

By taking Eq. (2) into account, Eq. (10) becomes

$$S_2^I = \frac{F_{ub}(\delta_s - 1)}{\cos\theta} \tag{11}$$

Hence, after an estimation of F_{ub} by means of Eq. (1) and an evaluation of δ_s by Eq. (3) the strength of the equivalent strut can be obtained.

In order to consider the coupling between frame and infill the strength of the infilled frame can be more correctly evaluated by substituting the strength of the strut S_2^I in Eq. (9) with a fictitious strength S_2 which, summed with the strength of the bare frame, allows one to obtain the strength of the infilled frame exactly. The parameter ω_S that makes it possible to change S_2^I into S_2, namely to write

$$\omega_S = \frac{S_2}{S_2^I} \tag{12}$$

is here estimated by means of experimental observations. In Fig. 22 it is proposed a correlation between the parameter α_S, defining the ratio between the horizontal component of the conventional diagonal strength of an infill F_{up} and the corresponding bare frame strength F_{ub} and the value of ω_S. This tool allows one to obtain the fictitious strength S_2 of an infill panel.

It can be observed that the dependence of ω_S on the ratio α_S can be fitted by the equation:

$$\omega_S = 0.90\alpha_s^{0.26} \tag{13}$$

Hence if α_S is known, ω_S, δ_S and S_2 can also be obtained. Eq. (13) makes it possible to predict the fictitious strength to be attributed to the equivalent strut and to make more accurate Eq. (9) and all derived analytical expressions.

The strength envelope was finally defined as reported in Cavaleri et al. [26], only depending on the parameters α, β and ζ. The initial stiffness (branch I) was defined as

$$K_1 = \frac{E_d t w}{d} \tag{15}$$

The stiffness in branch II was related to the parameter β as:

$$K_2 = \beta K_1 \tag{16}$$

Once the peak strength S_2 was assigned, the yielding strength S_1 was defined through the parameter α as

$$S_1 = \alpha S_2 \tag{17}$$

The yielding and peak displacements were therefore directly identified

$$\delta_1 = S_1/K_1; \quad \delta_2 = \delta_1 + (S_2 - S_1)/K_2 \tag{18}$$

The softening branch was linearized by connecting the points S_2–δ_2 and S_3–δ_3 (branch III), since $S_3 = 0.7\ S_2$, and δ_3 was obtained by the following expression [26]:

$$\delta_3 = \frac{1}{\zeta}\ln\left[\frac{S_2}{S_3}\exp(\zeta\delta_2)\right] \tag{19}$$

The calibration of the parameters α, β and ζ, which characterize the envelope curve, were provided for each infill typology by using the results of pushover analyses on the different types of systems tested. The values selected for the α, β and ζ are those that allow the best fitting of the pushover curves on the mean experimental strength envelopes for each specimen typology. The pushover curves, used for the calibration of the equivalent strut model law, are reported in Fig. 23 All properties that identify the equivalent struts are summarized in Table 6.

3.3. Model validation: experimental/analytical comparisons

Simulations of the tests were carried out by assigning as input the displacement history actually applied at the top of each specimen. The calibration of the parameter α_2 which defines the fundamental Pivot point P_3 was performed, for each of the 3 typologies of infilled frames, by the execution of several trial analyses. The values selected for α_2, which gave the best fitting of the experimental results, are shown in Table 6 and are also suggested for masonry infill typologies having similar characteristics.

In Figs. 24–26 experimental/analytical comparisons of the cyclic force–displacement responses of 3 different specimens, one for each infill/frame typology, are shown.

By observation of the cycle shapes, the results appear to be acceptable for each of the three cases. Regarding the experimental/analytical strength and stiffness matching, the role of the correct prediction of the strength envelope, which guides the cycles, appears to be fundamental to obtain reliable results. The more relevant differences in terms of strength and stiffness with respect to the experimental results are limited to a restricted number of cycles and do not exceed 15% for the strength and 20% for the stiffness. The consistency of the Pivot model becomes more evident observing the experimental/analytical responses obtainable by developing the lateral displacements (Figs. 27–29), that is by plotting the force versus the distance covered by the top of each frame.

As final reference for the validation, a comparison in terms of dissipated energy was carried out. For both real experimental tests and simulations by means of the Pivot model, the energy dissipated by each cycle, respectively W_e and W_p, and the cumulative dissipated energy, respectively ΣW_e and ΣW_p, were calculated. The comparisons are shown in Figs. 30–32. The energy dissipation, evaluated at each cycle analyzing the simulations, shows good correspondence with the effective experimental dissipation. The comparison in terms of cumulative energy dissipation also shows that the global experimental behavior is well fitted, demonstrating

the good reliability in predicting also global dissipative capacities. The normalized cumulative energy dissipation was also calculated dividing this dissipation by the term ΣD, which represents the

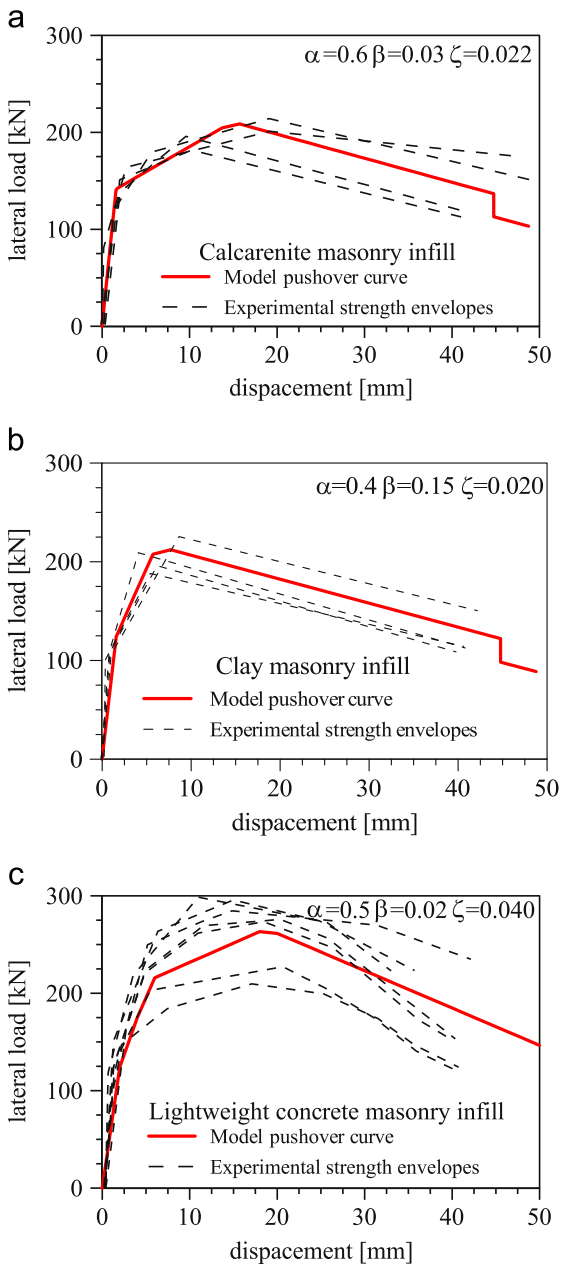

Fig. 23. Calibration of parameters trough best pushover-fitting curves. (a) calcarenite masonry infill; (b) clay masonry infill; and (c) lightweight concrete masonry infill.

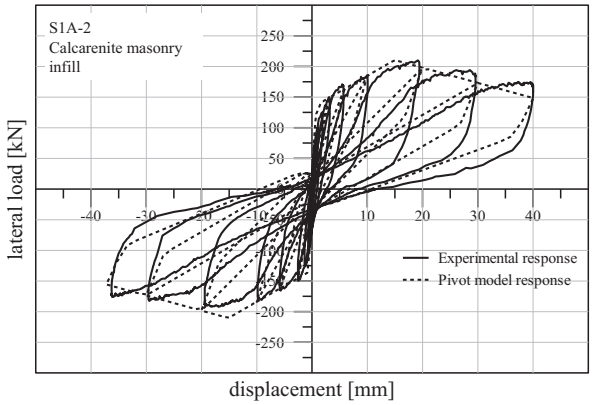

Fig. 24. Experimental/analytical cyclic response for a calcarenite masonry infilled frame specimen.

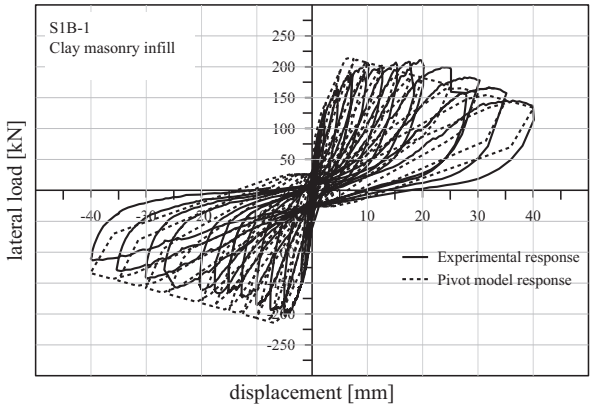

Fig. 25. Experimental/analytical cyclic response for a clay masonry infilled frame specimen.

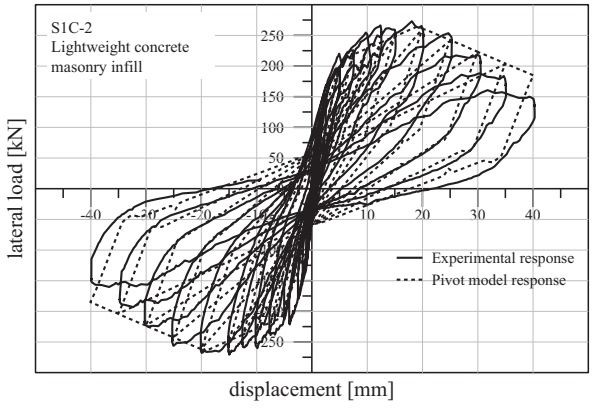

Fig. 26. Experimental/analytical cyclic response of lightweight for a concrete masonry infilled frame specimen.

Table 6
Identification parameters for the equivalent struts.

Infill of	Dimensionless cross section	Strength envelope axial force–displacements law values			Strength envelope parameters			Pivot hysteretic parameters
	w/d	S_1 [kN] δ_1 [mm]	S_2 [kN] δ_2 [mm]	S_3 [kN] δ_3 [mm]	α	β	ζ	α_2
Calcarenite	0.39	148 0.50	248 11.6	173 27.8	0.60	0.030	0.022	0.10
Clay	0.30	101 0.40	254 4.44	178 22.3	0.40	0.150	0.020	0.25
LW concrete	0.32	98 0.28	196 14.2	138 23.1	0.50	0.020	0.040	0.05

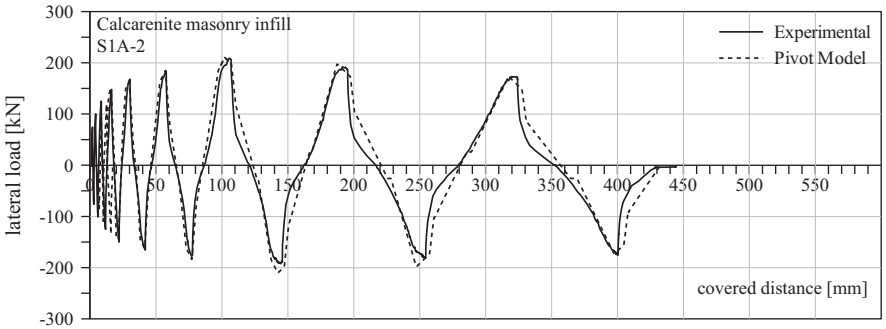

Fig. 27. Experimental/analytical force-lateral covered distance comparison test for a calcarenite masonry infilled frame specimen.

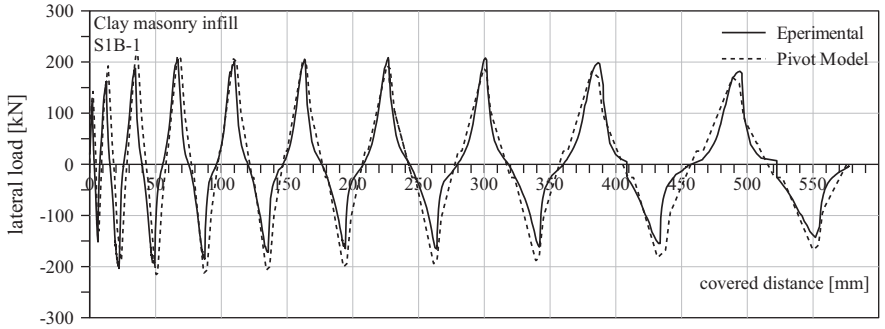

Fig. 28. Experimental/analytical force-lateral covered distance comparison test for a clay masonry infilled frame specimen.

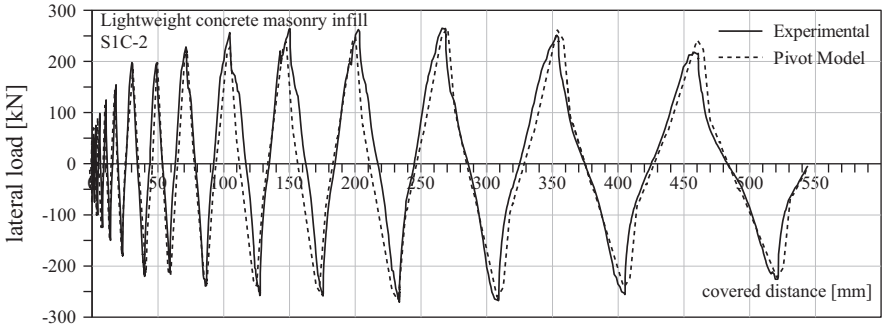

Fig. 29. Experimental/analytical force-lateral covered distance comparison test for a lightweight concrete masonry infilled frame specimen.

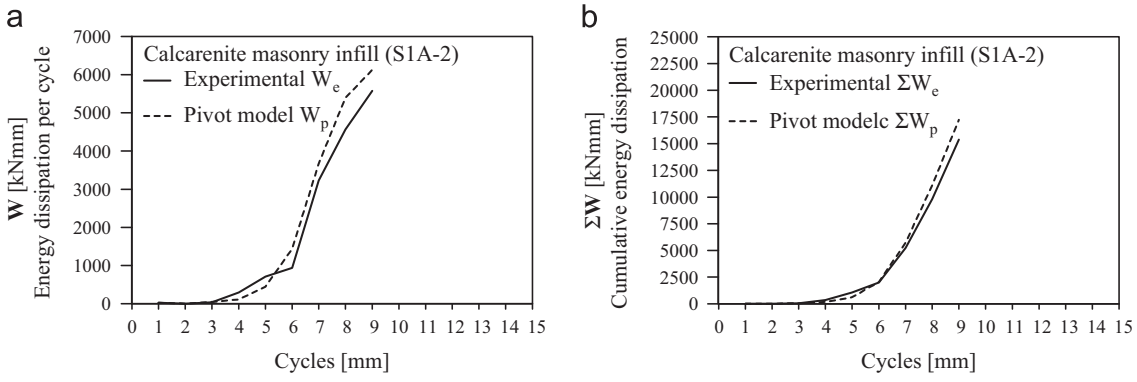

Fig. 30. Experimental/analytical energy dissipation comparison. (a) Energy dissipation per cycle; and (b) Cumulative energy dissipation. S1A-2 specimen.

cumulative sum of the displacements, giving information about the energy dissipation capacities of the single infill/frame systems. The frames infilled with lightweight concrete masonry and calcarenite masonry seem to have the best dissipative properties with respect to the frames infilled with clay masonry. The energy dissipation values and the prediction errors are summarized in Table 7.

3.4. Application of the pivot model to a case nonlinear TH analysis of a multi-story multi-bay frame

As an example of application of the proposed pivot law, a nonlinear time history analysis of a multi-story multi-bay infilled frame prototype structure has been carried out and compared with the corresponding bare frame structure. The 2D frame

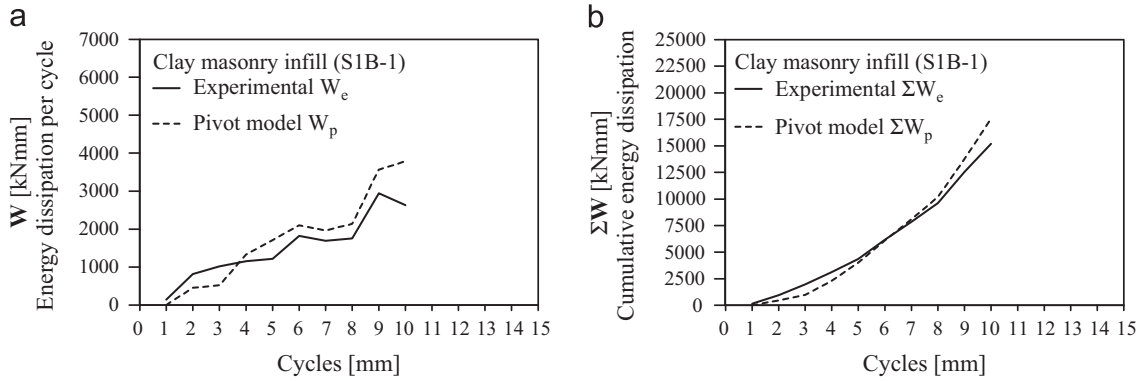

Fig. 31. Experimental/analytical energy dissipation comparison. (a) Energy dissipation per cycle; and (b) Cumulative energy dissipation. S1B-1 specimen.

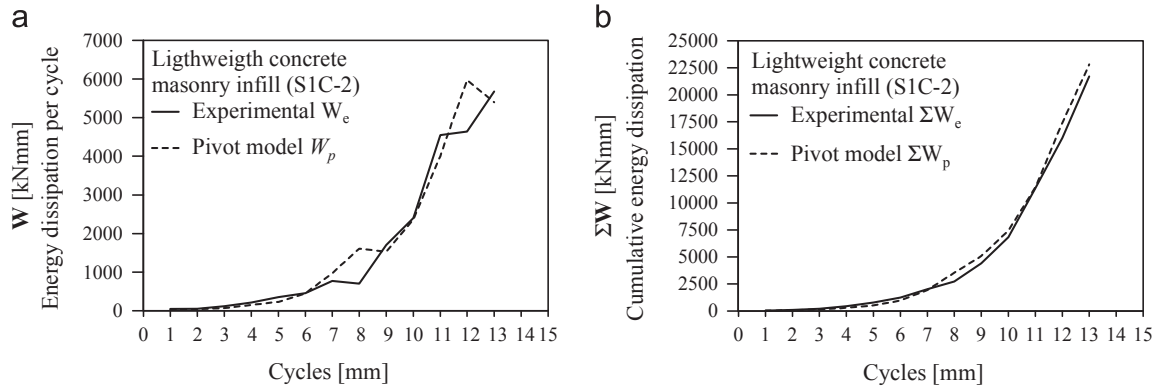

Fig. 32. Experimental/analytical energy dissipation comparison. (a) Energy dissipation per cycle; and (b) Cumulative energy dissipation. S1C-2 specimen.

Table 7
Experimental/analytical comparison of dissipated energy and percentage of error.

Specimen	ΣD [mm] Cumulative displacements	Experimental		Pivot model		$(\Sigma W_p - \Sigma W_e)/\Sigma W_e$ [%] Model prediction error
		ΣW_e [kN mm] Cumulative dissipated energy	$\Sigma W_e/\Sigma D$ [kN mm/mm] Normalized cumulative dissipated energy	ΣW_p [kN mm] Cumulative dissipated energy	$\Sigma W_p/\Sigma D$ [kN mm/mm] Normalized cumulative dissipated energy	
S1A-2 (Calcarenite)	430	15,369.4	35.74	17,242.4	40.10	+12.2
S1B-1 (Clay)	580	15,185	26.18	17,561	30.28	+15.6
S1C-2 (LW concrete)	550	21,697	39.45	22,810	41.47	+5.1

structure was characterized by four story and two bays. The geometric characteristics are shown in Fig. 33. A lumped plasticity model was employed to model RC member plastic hinging, while the nonlinear Pivot law was assigned to the equivalents struts. Considering the different shape of the frame bays, two different equivalent struts were identified, each one with a proper force–displacement law (Table 8). The different height of the first story with respect to the upper ones was instead neglected in the identification process.

A uniform load of 40 kN/m was assigned to the beams in order to simulate the presence of a floor in an ordinary case. Concrete and steel rebars strengths were fixed as 25 MPa and 450 MPa respectively. For the calibration of plastic hinges an ultimate concrete strain of 0.6% was considered. The panels were supposed to be constituted by clay masonry characterized by $f_{v0m}=0.4$ MPa and thickness 200 mm.

As external input the El Centro ground motion record was chosen (Fig. 34). The analyses showed the different behavior of the structure with and without infills. The greater stiffness of the infilled structure produced an increase of recorded base shear and reduced interstory drifts (Figs. 35–37). The ground motion acceleration spectrum was compared with the resulting pseudo acceleration spectra at the roof level in both the considered cases (Fig. 38). As the figure shows, a restricted range of dominant frequencies can be recognized for the infilled structure, differently from the larger one associated to the motion of the bare structure. This is the consequence of a regularization of the motion caused by the presence of infills that strongly influence the overall stiffness. Regarding to the cyclic behavior of the infilled structure, the activation of the hysteretic mechanisms resulted to be delayed whit respect to the cycle shapes observed for bare frames (Fig. 39). This fact is associated to a different distribution of the plasticized zones on the frame (Fig. 40) that are also largely reduced in terms of quantity of activated hinges. This is due to the higher overall strength given by the infills which attract on themselves the most of the seismic action acting on the structure modifying the expected damage mechanisms.

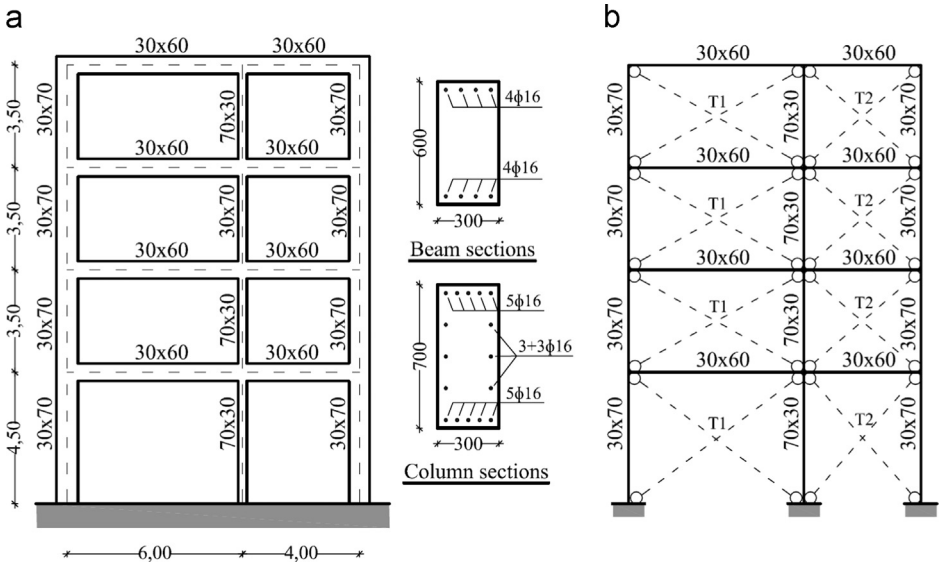

Fig. 33. Prototype structure. (a) geometry and cross section features; and (b) model of the infilled/bare frame.

Table 8
Mechanical features and Pivot points for the masonry infills used in the prototype structure.

Shear strength and thickness of infills	
f_{v0m} [Mpa]	t [mm]
0.40	200

Force–displacement Pivot envelope			
Rectangular frames		Square frames	
F [kN]	δ [mm]	F [kN]	δ [mm]
F_1–δ_1 154.0	0.55	F_1–δ_1 122.0	0.52
F_2–δ_2 386.0	2.6	F_2–δ_2 168.0	1.68
F_3–δ_3 270.0	14.0	F_3–δ_3 214.0	13.5

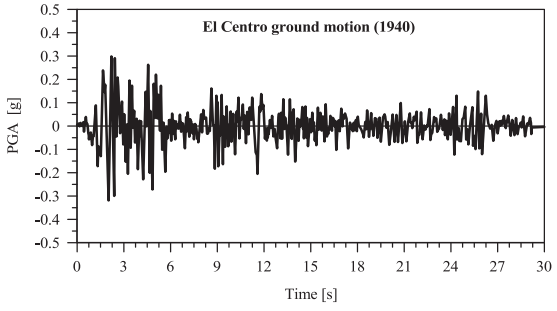

Fig. 34. Ground motion record used for the analyses (El Centro, 1940).

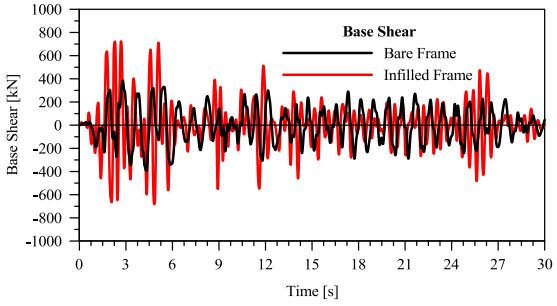

Fig. 35. Infilled and bare frame. Base shear vs. time.

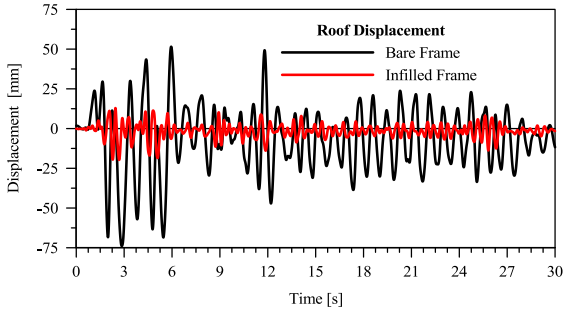

Fig. 36. Infilled and bare frame. Roof displacement vs. time.

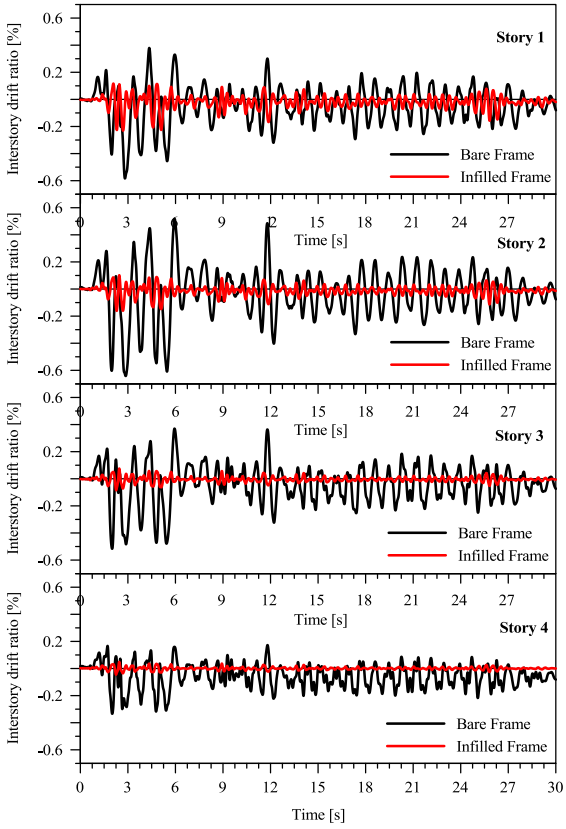

Fig. 37. Infilled and bare frame. Interstorey drifts.

4. Conclusions

An experimental campaign on the cyclic response of RC fully infilled frames arranged with 3 different kinds of masonry infills has been discussed in this paper, evidencing the influence of infill panels on strength, stiffness and ductility. By the observation of the experimental results a strategy for the assessment of the cyclic response of infilled frames systems has been developed, identifying the Pivot hysteretic model as a simple analytical cyclic law that can be employed to perform nonlinear time history analyses. In fact the Pivot model has been proved to be suitable for the equivalent diagonal struts used to include infill effects in structural models. Basing on the experimental and the analytical studies here described, considering that the presence of infills produces a significant modification of the behavior of frames, the following was concluded:

(1) An adaptation of the Pivot hysteretic model for the analytical evaluation of the cyclic response of infilled frames structures is possible and radically simplifies the modeling approach, being the Pivot model governed by only one parameter (α_2); the computational effort is also reduced since the Pivot model is based on a few geometric rules rather than analytical laws;
(2) the identification of the parameters α_2 which defines the degrading of the Pivot cycles, for the masonry infills involved in this study, gave optimal results, and experimental/analytical comparisons of the responses showed good reliability in the prediction of the responses themselves: limited differences of strength and stiffness with respect to the experimental tests were observed; further, dissipation energy comparisons revealed good matching with very limited overestimations;
(3) the definition of the strength, the ultimate deformability and the stiffness, which are necessary in order to define the Pivot model, can be obtained using approaches already available in the literature; this confirms the versatility of the Pivot model;
(4) taking into account the results of the present study, the application of the model is suggested when it is necessary to assess the global response in terms of displacements, ductility and energy dissipation in nonlinear time history analyses;
(5) considering the uncertainties related to the number of specimens, the scale effects and the variability of different masonries' mechanical properties, further experimental/analytical studies involving different infill/frame couplings are desirable; and

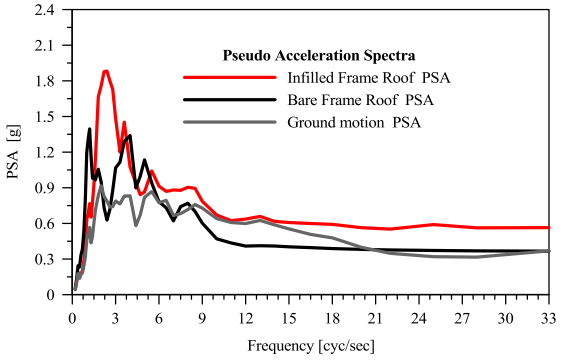

Fig. 38. Pseudo acceleration spectra for ground motion, roof bare frame and roof infilled frame.

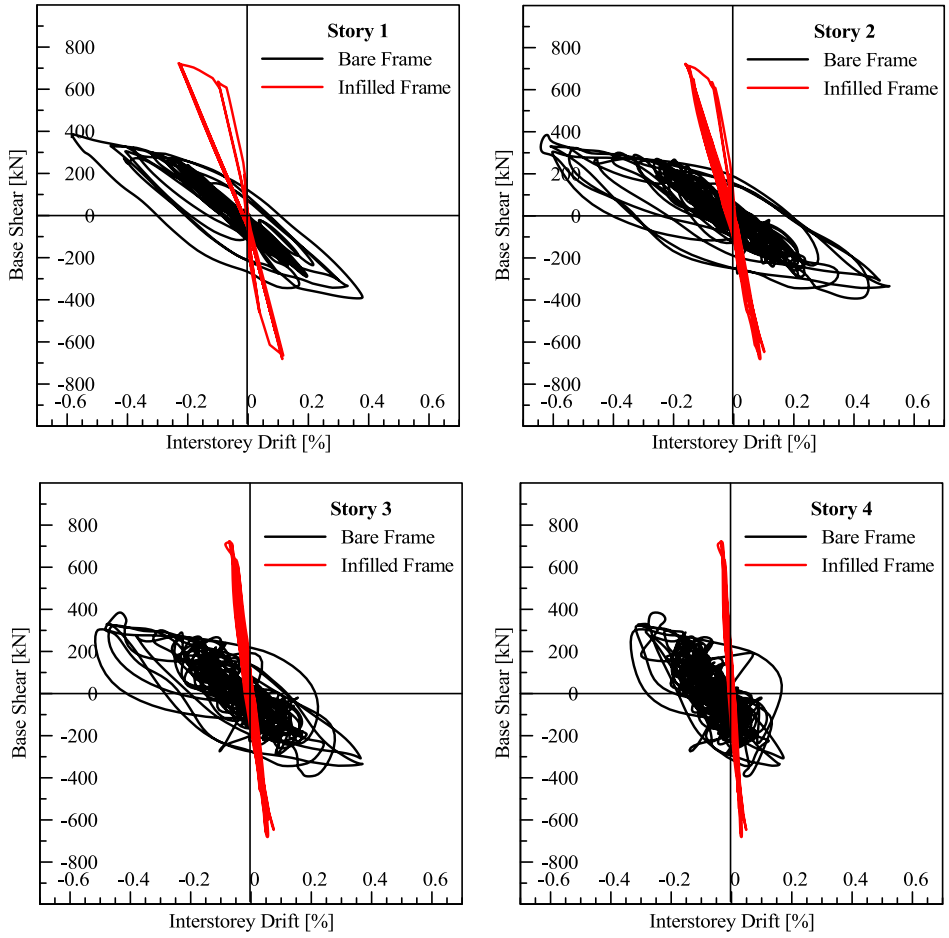

Fig. 39. Infilled and bare frame. Base shear vs. interstorey drift.

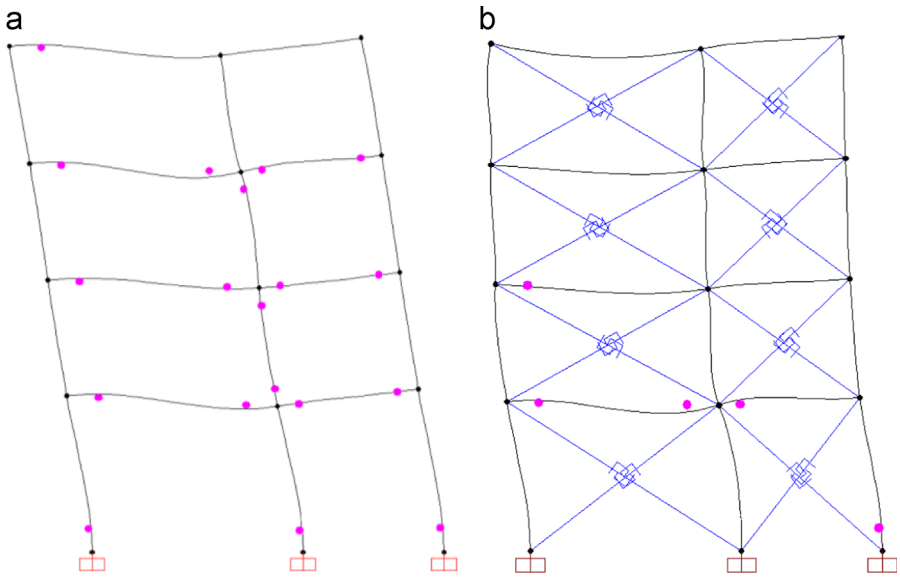

Fig. 40. Hinges yielding at the end of the ground motion. (a) bare frame; and (b) infilled frame.

(6) this work, besides the enlargement of the experimental knowledge on cyclic behavior of RC infilled frames, is aimed to demonstrate that a simple modeling of equivalent struts is possible by means of the Pivot hysteretic model; the values suggested for the α_2 parameter are relative to the masonry infill typologies involved in the discussed experimental campaign, anyway each user can perform a proper calibration if needed on the basis of its own experimental results and sensitivity.

Acknowledgments

This study was sponsored by ReLUIS, Rete di Laboratori Universitari di Ingegneria Sismica, Linea 2, Obiettivo 5: Influenza della Tamponatura sulla Risposta Strutturale.

References

[1] FEMA. NEHRP Guidelines for the seismic rehabilitation of buildings. FEMA 273, Washington, DC;1997.
[2] Holmes M. Steel frames with brickwork and concrete infilling. In: Proceedings of Institution of Civil Engineers, paper No. 6501; 1961. p. 473–8.
[3] Stafford Smith B. Behaviour of the square infilled frames. Struct Div (ASCE) 1966;92(1):381–403.
[4] Stafford Smith B, Carter C. A method for analysis for infilled frames. In: Proceedings of Institution of Civil Engineers, paper No. 7218; 1969. p. 31–48.
[5] Mainstone RJ. Supplementary note on the stiffness and strength of infilled frames, current paper CP 13/74, UK: Building Research Station;1974.
[6] Dawe JL, Seah CK. Analysis of concrete masonry infilled steel frames subjected to in-plane loads. In: Proceedings of the 5th Canadian masonry symposium, Vancouver; 1989. p. 329–40.
[7] Durrani AJ, Luo YH. Seismic retrofit of flat-slab buildings with masonry infill. In: Proceedings of the NCEER workshop on seismic response of masonry infills, report NCEER-94-0004; 1994.
[8] Saneinejad A, Hobbs B. Inelastic design of infilled frames. J Struct Eng (ASCE) 1995;121(4):634–50.
[9] Papia M, Cavaleri L, Fossetti M. Infilled frames: developments in the evaluation of the stiffening effect of infills. Struc Eng Mech 2003;16(6):675–93.
[10] Amato G, Cavaleri L, Fossetti M, Papia M. Infilled frames: influence of vertical loads on the equivalent diagonal strut model. In: Proccedings of the XIV WCEE, Beijing; 2008.
[11] Amato G, Fossetti M, Cavaleri L, Papia M. An updated model of equivalent diagonal strut for infill panels. In: Workshop: Quali Prospettive per l'Eurocodice 8 alla Luce delle Esperienze Italiane, Napoli; 2009.
[12] Cavaleri L, Papia M. A new dynamic identification technique: application to the evaluation of the equivalent strut for infilled frames. Eng Struct 2003;25(7) (889–01).
[13] Cavaleri L. Identification of stiffness, dissipation and input parameters of randomly excited non-linear systems: capability of Restricted Potential Models (RPM). Int J Non-Linear Mech 2006;41(9):1068–83.
[14] Benfratello S, Cavaleri L, Papia M. Identification of stiffness, dissipation and input parameters of multi degree of freedom civil systems under unmeasured base excitations. Prob Eng Mech 2009;24(2):190–8.
[15] Cavaleri L, Papia M. An output-only stochastic parametric approach for the identification of linear and nonlinear structures under random base excitations: advances and comparisons. Prob Eng Mech 2014;35:11–21.
[16] Panagiotakos TB, Fardis MN. Seismic response of infilled RC frames structures. In: Proceedings of the XXI WCEE, Acapulco, Mexico; 1996.
[17] Bertoldi SH, Decanini LD, Gavarini C Telai tamponati soggetti ad azioni sismiche, un modello semplificato: confronto sperimentale e numerico. In: Atti del 6 Convegno Nazionale ANIDIS, 2, Perugia; 1993. p. 815–24.
[18] Klingner RE, Bertero VV. Earthquake resistance of infilled frames. J Struct Eng (ASCE) 1978;104(6):973–89.
[19] Doudoumis IN, Mitsopoulou EN. Non-linear analysis of multi-storey infilled frames for unilateral contact condition. In: Proceedings of the 8th European conference on earthquake engineering, 3, Lisbon; 1986. p. 63–70.
[20] Mander JB, Nair B, Wojtkowski K, Ma J. Experimental study on the seismic performance of brick infilled steel frames with and without retrofit. Technical report. Buffalo: NCEER; 1993 (93-0001).
[21] Mander JB, Nair B. Seismic resistance of brick infilled steel frames with and without retrofit. Mason J 1994;12(2):24–37.
[22] Mehrabi AB, Benson Shing P, Schuler MP, Noland JL. Experimental evaluation of masonry-infilled RC frames. J Struct Eng (ASCE) 1996;122(3):228–37.
[23] Madan A, Reinhorn AM, Mander JB, Valles RE. Modeling of masonry infill panels for structural analysis. J Struct Eng (ASCE) 1997;123(10):1295–302.
[24] Crisafulli FJ. Seismic behaviour of reinforced concrete structures with masonry infills [Ph.D. thesis]. 1997.
[25] Kappos AJ, Stylianidis KC, Michaildis CN. Analytical models for brick masonry infilled R/C frames under lateral loading. J Earthq Eng 1998;2(1):59–87.
[26] Cavaleri L, Fossetti M, Papia M. Infilled frames: developments in the evaluation of cyclic behaviour under lateral loads. Struct Eng Mech 2005;21(4):469–94.
[27] Crisafulli FJ, Carr AJ. Proposed macro-model for the analysis of infilled frame structures. Bull N Z Soc Earthq Eng 2007;40(2):69–77.
[28] Asteris PG, Antoniou ST, Sphianopulos DS, Chrysostomou CZ. Mathematical macromodeling of infilled frames: state of the art. J Struct Eng (ASCE) 2011;137(12):1508–17.
[29] Asteris PG. Lateral stiffness of brick masonry infilled plane frames. J Struct Eng (ASCE) 2003;129(8):1071–9.
[30] Dolšek M, Fajfar P. The effect of masonry infills on the seismic response of four storey reinforced concrete frame–a deterministic assessment. Eng Struc 2008;30(7) (1991–001).
[31] Kakaletsis DJ, Karayannis CG. Experimental investigation of infilled reinforced concrete frames with openings. Struct J (ACI) 2009;106(2):132–41.
[32] Stavridis A, Koutromanos I, Benson Shing P. Shake-table tests of a three-story reinforced concrete frame with masonry infill walls. Earthq Eng Struct Dyn 2012;41(6):1089–108.
[33] Uva G, Porco F, Fiore A. Appraisal of masonry infill walls effect in the seismic response of RC framed buildings: a case study. Eng Struct 2012;34:514–26.
[34] Fiore A, Netti A, Monaco P. The influence of masonry infill on the seismic behaviour of RC frame buildings. Eng Struct 2012;44:133–45.

[35] Dowell RK, Seible F, Wilson EL. Pivot Hysteresis model for reinforced concrete members. Struct J (ACI) 1998;95(5):607–17.
[36] Cavaleri L, Di Trapani F, Macaluso G, Papia M. Reliability of code-proposed models for assessment of masonry elastic moduli. Ing Sism 2012;29(1):38–59.
[37] Shing PB, Stavridis A. Analysis of seismic response of masonry-infilled rc frames through collapse. ACI Struct J 2014 (297–297).
[38] Koutromanos I, Stavridis A, Benson Shing P, Willam K. Numerical modeling of masonry-infilled RC frames subjected to seismic loads. Comput Struct 2011;89(11–12):1026–37.
[39] Takeda T, Sozen MA, Nielsen NN. Reinforced concrete response to simulated earthquakes. J Struct Div (ASCE) 1970;96(ST12):2557–73.
[40] Cavaleri L, Di Trapani F, Macaluso G, Colajanni P. Definition of diagonal Poisson's ratio and elastic modulus for infill masonry walls. Mater Struct 2014;47(1-2):239–62.